Silicon-on-insulator guided mode resonance grating for evanescent field molecular sensing

Schmid, J. H.; Sinclair, W.; García, J.; Janz, S.; Lapointe, J.; Poitras, D.; Li, Y.; Mischki, T.; Lopinski, G.; Cheben, P.; Delâge, A.; Densmore, A.; Waldron, P.; Xu, D.-X.

Publisher's version / Version de l'éditeur:
https://doi.org/10.1364/OE.17.018371
Optic Express, 17, 20, pp. 18371-18380, 2009

Silicon-on-insulator guided mode resonant grating for evanescent field molecular sensing

J. H. Schmid,[1,*] W. Sinclair,[1] J. García,[2] S. Janz,[1] J. Lapointe,[1] D. Poitras,[1] Y. Li,[3] T. Mischki,[3] G. Lopinski,[3] P. Cheben,[1] A. Delâge,[1] A. Densmore,[1] P. Waldron,[1] and D.-X. Xu[1]

[1]*Institute for Microstructural Sciences, National Research Council Canada, Ottawa, Ontario, K1A 0R6*
[2]*Valencia Nanophotonics Technology Center, Universidad Politécnica de Valencia, 46022 Valencia, Spain*
[3]*Steacie Institute for Molecular Sciences, National Research Council Canada, Ottawa, Ontario, K1A 0R6*
[*]*Corresponding author: jens.schmid@nrc-cnrc.gc.ca*

Abstract: We present experimental and theoretical results of label-free molecular sensing using the transverse magnetic mode of a 0.22 μm thick silicon slab waveguide with a surface grating implemented in a guided mode resonance configuration. Due to the strong overlap of the evanescent field of the waveguide mode with a molecular layer attached to the surface, these sensors exhibit high sensitivity, while their fabrication and packaging requirements are modest. Experimentally, we demonstrate a resonance wavelength shift of ~1 nm when a monolayer of the protein streptavidin is attached to the surface, in good agreement with calculations based on rigorous coupled wave analysis. In our current optical setup this shift corresponds to an estimated limit of detection of 0.2% of a monolayer of streptavidin.

OCIS codes: (130.6010) Sensors; (130.3120) Integrated optics devices; (230.5750) Resonators; (050.2770) Gratings;

References and links

1. J. Homola, S. S. Yee, G. Gauglitz, "Surface plasmon resonance sensors: review," Sensors and Actuators B **54** (1) 3–15 (1999).
2. A. Densmore, D.-X. Xu, S. Janz, P. Waldron, T. Mischki, G. Lopinski, A. Delâge, J. Lapointe, P. Cheben, B. Lamontagne, and J. H. Schmid, "Spiral-path high-sensitivity silicon photonic wire molecular sensor with temperature-independent response," Opt. Lett. **33** (6) 596-598 (2008).
3. D.-X. Xu, A. Densmore, A. Delâge, P. Waldron, R. McKinnon, S. Janz, J. Lapointe, G. Lopinski, T. Mischki, E. Post, P. Cheben, and J. H. Schmid, Opt. Express **16** (19), 15137-15148 (2008).
4. A. Densmore, D.-X. Xu, P. Waldron, S. Janz, P. Cheben, J. Lapointe, A. Delâge, B. Lamontagne, J.H. Schmid, and E. Post, "A silicon-on-insulator photonic wire based evanescent field sensor," IEEE Photon. Technol. Lett. **18** (23) 2520-2522 (2006).
5. S. S. Wang, R. Magnusson, and J. S. Bagby, "Guided mode resonances in planar dielectric-layer diffraction gratings," J. Opt. Soc. Am. A **7** (8) 1470-1474 (1990).
6. J. J. Wang, L. Chen, S. Kwan, F. Liu, and X. Deng, "Resonant grating filters as refractive index sensors for chemical and biological detections," J. Vac. Sci. Technol. B **23** (6) 3006-3010 (2005).
7. The RODIS software package, developed by the Photonics Research Group at the University of Ghent, Belgium, is available for download from the website: http://www.photonics.intec.ugent.be/research/facilities/design/rodis/default.htm
8. M. G. Moharam and T. K. Gaylord, "Rigorous coupled-wave analysis of planar-grating diffraction", J. Opt. Soc. Am. **71** (7), 811-818 (1981).
9. I. M. White and X. Fan, "On the performance quantification of resonant refractive index sensors," Opt. Express **16** (2) 1020-1028 (2008).
10. J. Hu, X. Sun, A. Agarwal, and L. C. Kimerling, "Design guidelines for optical resonator biochemical sensors", J. Opt. Soc. Am. B **26** (5) 1032-1041 (2009).
11. D. W. Peters, S. A. Kemme, and G. R. Hadley, "Effect of finite grating, waveguide width, and end-facet geometry on resonant subwavelength grating reflectivity," J. Opt. Soc. Am. A **21** (6) 981-987 (2004).
12. K. De Vos, I, Bartolozzi, E, Schacht, P. Bienstman, and R. Baets, "Silicon-on-insulator microring resonator for sensitive and label-free biosensing," Opt. Express **15** (12), 7610-7615 (2007).

13. A. Delâge, D.-X. Xu, R. W. McKinnon, E. Post, P. Waldron, J. Lapointe, C. Storey, A. Densmore, S. Janz, B. Lamontagne, P. Cheben, and J. H. Schmid, "Wavelength-dependent model of ring resonator sensor excited by a directional coupler," J. Lightw. Technol. **27** (9) 1172-1180 (2009).
14. J. Heebner, R. Grover, and T. Ibrahim, "Optical microresonators: theory, fabrication, and applications," Springer Series in Optical Sciences **138**, Springer, New York (2008).

1. Introduction

The development of new label-free optical molecular sensing technologies is an active field of both academic and industrial research. Such techniques are needed for the study of affinity binding reactions between matching molecular pairs, e.g. complementary DNA strands or antibody-antigen pairs. Generally, sensors make use of a functionalized substrate surface, on which one component of the molecular pair has been immobilized. The binding of the matching component then leads to a surface modification that can be detected optically.

Currently, surface plasmon resonance (SPR) is the most widely accepted method for carrying out label-free molecular binding studies [1]. SPR uses the interaction of the evanescent field of a surface plasmon in a thin functionalized gold film with a molecular layer that attaches to the surface. This interaction causes a shift of the plasmon resonance frequency, which is typically detected as the angular shift of a minimum in the specular reflectivity of a prism coupled laser beam. The sensitivity of an SPR sensor is limited fundamentally by the short propagation length of the surface plasmons of ~ 20 μm, which leads to a broad spectral or angular width of the optical signal.

An alternative label-free optical sensing technique uses the evanescent field of a dielectric or semiconductor waveguide to sense changes at the functionalized waveguide surface caused by molecular binding events. In recent years, we have developed very sensitive silicon photonic wire evanescent field (PWEF) sensors in Mach-Zehnder interferometer (MZI) [2] and ring resonator [3] configurations. In particular, for infrared light with a wavelength of λ = 1.55 μm the transverse magnetic (TM) mode of a 0.22 μm thick silicon waveguide provides the highest surface sensitivity of all common waveguide material platforms [4]. A detection limit as low as ~160 fg/mm^2 of protein mass density on the waveguide surface was demonstrated. While the concept of waveguide evanescent field sensors is not new, using the high index contrast silicon-on-insulator (SOI) platform greatly enhances the capability of this technology. The optimized sensitivity results from the large overlap of the evanescent electric field of the waveguide mode with the surface layer due to the electromagnetic boundary conditions.

The PWEF sensors offer remarkably high sensitivity, but optical coupling and packaging requirements of photonic wire chips are demanding. Alternatively, one can use a surface grating to interrogate a silicon slab waveguide sensor. In this case the optical layout of the sensor system is almost identical to that used in SPR systems, with a free space laser beam incident on the sample from above or below the substrate. A similar configuration has been used in guided mode resonance filters to achieve very narrow spectral response [5]. When used as a molecular sensor, the transduction signal may again be either the angle or wavelength shift of the guided mode resonance in response to a refractive index change at the surface [6]. By the same arguments used for the PWEF sensors, choosing the TM mode of a thin SOI slab waveguide maximizes the sensitivity of guided mode resonance grating sensors.

The basic configuration of an SOI resonant grating sensor with optimized silicon layer thickness is shown in Fig. 1. The structure consists of a thin SiO_2 surface grating on an SOI substrate with a 0.22 μm thick silicon and a 3 μm thick buried oxide (BOX) layer. The silicon waveguide can be functionalized for sensor operation. Optical probing is done from the backside of the SOI wafer substrate (the top in Fig. 1) so as to not interfere with the delivery of analyte to the front sensing area. To facilitate probing, the substrate is polished on the backside and coated with an antireflective (AR) coating. The guided mode resonance, which occurs when the grating couples the incident beam to the slab waveguide mode, can be observed in the specular reflectivity spectrum. In this paper we describe theoretical and

experimental results on the performance of SOI resonant grating sensors. In particular, we use rigorous coupled wave analysis (RCWA) to calculate the change of the reflectivity spectra in response to surface modification by a thin organic layer. We discuss in detail the effect of finite grating size on the sensitivity and compare the results with MZI and ring resonator PWEF sensors. Finally, we present an experimental demonstration of a sensor using the biotin-steptavidin model binding system.

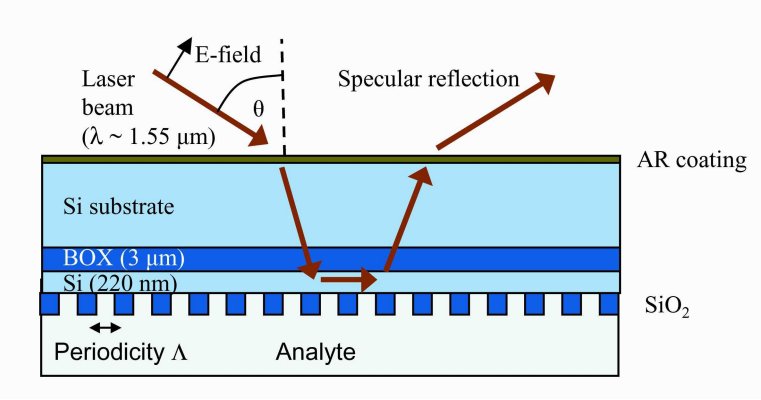

Fig. 1: Schematic side view of an SOI guided mode resonance sensor. At resonance, the laser beam incident from the wafer backside excites a slab waveguide mode in the thin silicon surface layer. The evanescent tail of this mode has a strong interaction with the sensor surface.

2. Theory and modeling

2.1 RCWA calculations of grating response

We have used the freely distributed "Rodis" RCWA software package [7] to calculate the reflectivity spectra of SOI resonant grating filters. In RCWA, both the incident and reflected light are assumed to be plane waves [8]. The modeled SOI layer structure is as shown in Fig. 1 with a 3 μm thick buried oxide (BOX) layer of refractive index n_{BOX} = 1.45 and a 0.22 μm thick silicon waveguide layer of index n_{Si} = 3.476. The grating material is SiO_2 with n_{SiO2} = 1.45. The condition for coupling the incident light to the waveguide can be expressed as $\beta = k_0 \sin\theta - k_g$, where $\beta = n_{eff} k_0$ is the waveguide propagation constant, $k_0 = 2\pi/\lambda$, $k_g = 2\pi/\Lambda$, λ is the free space wavelength of the light, Λ is the periodicity of the grating, θ is the angle of incidence as shown in Fig. 1 and n_{eff} is the slab waveguide effective index. From the coupling condition one can calculate the resonance wavelength:

$$\lambda = \Lambda\left(n_{eff} - \sin\theta\right) \qquad (1)$$

In our design the grating parameters are chosen such that the guided mode resonance occurs at λ = 1.55 μm for an angle of incidence of $\theta = 45°$.

The TM mode of the silicon waveguide is highly sensitive to refractive index changes in a thin layer at the waveguide surface [4]. To excite this mode, p-polarized light incident from the back surface of the sample with the electric field in the plane of incidence is used, as shown in Fig. 1. The AR coating on the back side is assumed to be perfect. Figure 2a shows the guided mode resonance for a 200 nm thick SiO_2 grating with a periodicity Λ = 1.24 μm and a duty ratio of 50%. The resonance feature is well defined with a reflectivity approaching unity. To estimate the sensitivity of the guided mode sensor to bulk refractive index changes, a series of reflection spectra are calculated for analyte material indices ranging from n_a = 1.0 to n_a = 1.3. The induced resonance wavelength shifts shown in Fig. 2a correspond to a

response of approximately 110 nm per refractive index unit (RIU). This shift is caused by the change of the effective index of the TM mode in the silicon slab waveguide, as predicted by Eq. (1). Figures 2b and 2c both show the response of the grating sensor in air (n_a = 1) with and without a 2 nm thick organic layer of refractive index n_{org} = 1.5 on the waveguide surface. The SiO_2 grating thickness is 50 nm for Fig. 2b and 200 nm for Fig. 2c. In both cases, the addition of the organic layer causes a wavelength shift of ~1 nm; however, the linewidth of the resonance is significantly increased for the 200 nm thick grating.

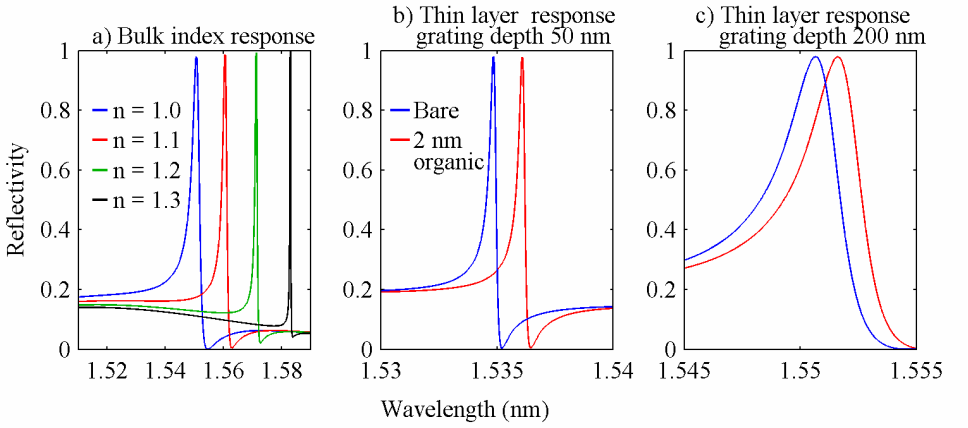

Fig. 2: RCWA calculations of resonant grating sensors. a) Response to bulk cladding index change. b) Resonance wavelength shift induced by the attachment of a 2 nm thick organic layer on a grating surface with periodicity Λ = 1.24 μm and a thickness of 50 nm in air. c) same as b) but for a grating with a thickness of 200 nm.

Figures 3a and 3b are analogous to Figs. 2b and 2c, but for a grating with a periodicity Λ = 1.17 μm and water cladding (n_a = 1.33). In this case, the addition of the organic layer causes a wavelength shift of only δλ ~ 0.5 nm. The wavelength shift is smaller than in air because of the smaller index difference between the organic layer and the cladding material that it replaces. As in the case of the air cladding, a trend of increased linewidth Δλ is observed for the thicker grating layer. For a resonant refractive index sensor, increased linewidth implies a decrease in performance. Recent studies have shown that when noise sources are taken into account, the limit of detection scales linearly with the linewidth over a wide range of sensor and noise parameters [9,10]. Therefore it is useful to introduce a sensitivity figure of merit (FOM) S as the ratio of the wavelength shift δλ induced by the addition of the thin molecular layer and the full width at half maximum (FWHM) of the resonance Δλ, as indicated in Fig. 3b. This quantity is plotted in Fig. 3c as a function of the grating depth. The strong increase of the sensitivity FOM for thin gratings is largely due to the decrease in linewidth.

The asymmetric shape of the Fano resonance features shown in Figs. 2 and 3 can be understood as the coherent superposition of the incident wave coupled to the waveguide by the grating, which has a Lorentzian spectral response, and the wave reflected by the multilayer with a slowly varying amplitude and phase across the spectral range of the resonance. The Lorentzian lineshape corresponds to an exponential temporal decay with a photon lifetime τ, which is inversely proportional to the resonance linewidth. In the context of this work, τ is the time the photon spends in the waveguide layer before being coupled out again by the grating. This lifetime is determined by the coupling of the waveguide mode to the radiation mode via the grating structure. Therefore a thin grating with a small coupling constant corresponds to a long photon lifetime and a narrow resonance. Likewise a weaker grating with a lower refractive index contrast between the grating and analyte materials will also exhibit a narrower resonance, as can be observed in the series of resonances shown in Fig. 2a. A long photon lifetime implies a large propagation distance $L = (c/n_{eff})\tau$ in the waveguide, where c is

the speed of light in vacuum and n_{eff} is the effective index of the waveguide mode. Based on the photon lifetime argument it can be shown that the observed linewidth scales as $\Delta\lambda \sim \lambda^2/L$. Therefore, to increase sensitivity by reducing the grating depth as suggested in Fig 2c, gratings with a larger area are required. This implies a trade-off between sensitivity and substrate size. Finite grating or beam size are not included explicitly in the RCWA model, which assumes a plane wave incident on a substrate of infinite dimensions. Finite size effects will be discussed in the following section.

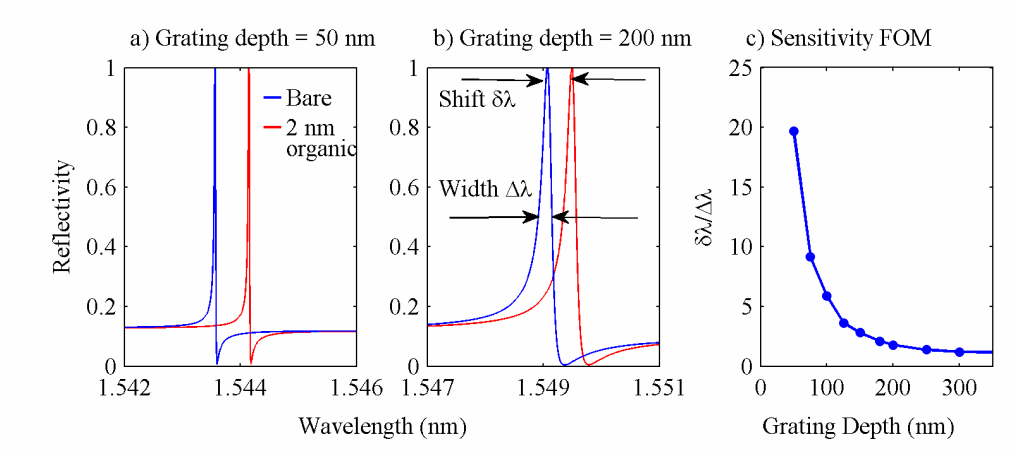

Fig. 3: a) Guided mode resonance wavelength shift induced by attachment of a 2 nm thick organic surface layer on a grating with periodicity Λ = 1.17 µm and a thickness of 50 nm in water. b) Same as a) for a grating with a thickness of 200 nm. c) Ratio of wavelength shift and linewidth (sensitivity figure of merit) as a function of grating depth.

2.2 Effect of grating size on sensitivity

The lateral extent of the grating determines the maximum beam diameter that can be used to excite the guided mode resonance. Here we consider a finite sized Gaussian beam incident on an infinite grating. It has been shown previously that additionally taking into account the finite size of the grating area does not affect the major conclusions of the following analysis [11]. Considering the wavelength dependence of the effective index, the angular dispersion of the resonance wavelength obtained from Eq. (1) can be expressed as:

$$\frac{\partial\lambda}{\partial\theta} = \frac{\Lambda\cos\theta}{\Lambda\dfrac{\partial n_{eff}}{\partial\lambda} - 1} \tag{2}$$

The angular spread of a Gaussian beam with waist size w_0 is given by $\Delta\theta = \lambda/(\pi w_0)$, which translates to a spread of the resonance wavelength of $\Delta\lambda = |\partial\lambda/\partial\theta|\,\Delta\theta$. Using Eq. (1) and (2) the following relation between the footprint $L = w_0/\cos\theta$ of the beam and the resonance linewidth can be derived:

$$\Delta\lambda = \frac{\lambda^2}{\pi L\left(n_g - \sin\theta\right)} \tag{3}$$

where n_g is the group index of the silicon waveguide. Interestingly, the same scaling $\Delta\lambda \propto \lambda^2/L$ applies as for the photon lifetime argument discussed in the previous section.

Since Eq. (3) gives an expression for the linewidth of the resonance, it can be used to calculate the sensitivity FOM. In order to derive an analytical expression, we consider the ratio of the wavelength shift induced by a change in the waveguide effective index δn_{eff} and

the linewidth, i.e. the quantity $S = \frac{1}{\Delta\lambda}\left(\frac{\delta\lambda}{\delta n_{eff}}\right)$. The shift $\delta\lambda$ can be calculated using Eq. (1) by considering a small change of the wavelength dependent effective index $n_{eff}(\lambda)$ with the following result:

$$\delta\lambda = \frac{\Lambda\delta n_{eff}}{1-\Lambda\frac{\partial n_{eff}}{\partial\lambda}} = \frac{\lambda\delta n_{eff}}{n_g - \sin\theta} \tag{4}$$

The second equality is obtained by using the resonance condition Eq. (1) to eliminate the periodicity Λ. Equations (3) and (4) can then be combined to obtain the expression for *S*:

$$S = \frac{1}{\Delta\lambda}\left(\frac{\delta\lambda}{\delta n_{eff}}\right) = \frac{\pi L}{\lambda} \tag{5}$$

This remarkably simple expression for the sensitivity FOM points again to the trade-off between sample size and ultimate limit of detection that can be achieved with a resonant grating sensor. In the derivation of Eq. (5) the response to a plane wave incident on the grating is implicitly assumed to be infinitely sharp, i.e. the linewidth broadening is entirely due to the angular spread of a Gaussian beam with a finite diameter. As seen in the previous section, however, even when exited by a plane wave of infinite extent, the guided mode resonance has a finite linewidth determined by the grating coupling strength. In order to optimize sensitivity, the grating strength must be chosen such that this intrinsic linewidth is of the same order as the size limited width in Eq. (3). This can be achieved using RCWA calculations. The sensitivity FOM *S* in Eq. (5) is expressed in terms of the change in effective index δn_{eff}. For a molecular sensor it is important to maximize the δn_{eff} induced by adsorption of a thin layer of target molecules on the surface. This problem is common to all evanescent field sensors and has been previously addressed. The result of this analysis led us to use a 0.22 μm thick silicon waveguide for our resonant grating sensors.

2.3 Performance comparison with photonic wire ring resonator and Mach-Zehnder interferometer sensors

The sensitivity FOM derived in the previous section can be compared to other configurations of evanescent field sensors. We consider in particular ring resonators and MZI sensors, which have also been implemented in thin SOI waveguides [2,3,12]. The transmission spectrum of a ring resonator is shown in Fig. 4a. It consists of a series of periodic dips with a spectral width $\Delta\lambda_{ring}$, which, in response to a change in the waveguide effective index δn_{eff}, shifts by an amount $\delta\lambda_{ring}$. This situation is analogous to the resonant grating sensor. Analytical expressions for $\Delta\lambda_{ring}$ and $\delta\lambda_{ring}$ have been previously derived [3,13,14]:

$$\delta\lambda_{ring} = \lambda\frac{\delta n_{eff}}{n_g} \tag{6a}$$

$$\Delta\lambda_{ring} = \frac{\lambda^2}{n_g LF} \tag{6b}$$

where *F* and *L* are the finesse and the length of the ring resonator, respectively. Using these expressions, one can show that the ring resonator sensitivity FOM is given by:

$$S_{ring} = \frac{1}{\Delta\lambda_{ring}}\left(\frac{\delta\lambda_{ring}}{\delta n_{eff}}\right) = \frac{LF}{\lambda} = \frac{\pi L_{eff}}{\lambda} \tag{7}$$

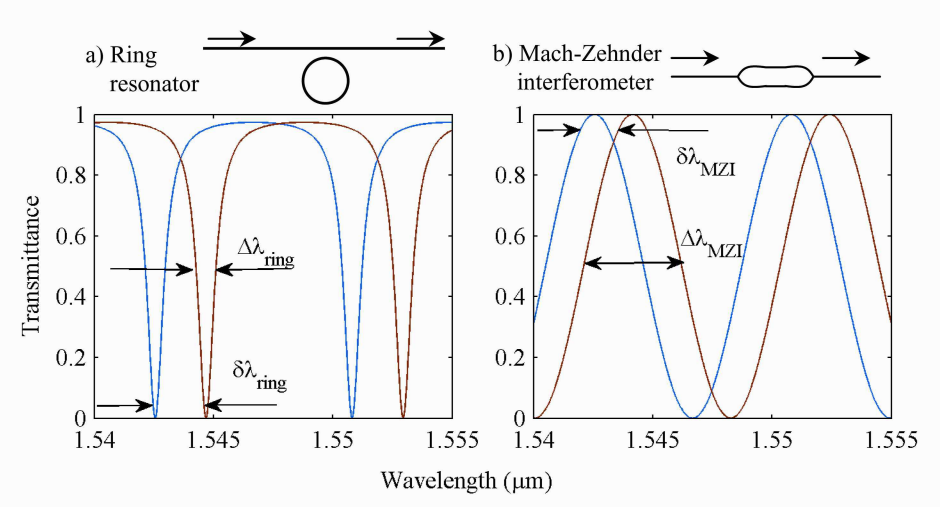

Fig. 4: Transmission spectra of ring resonator (finesse F = 10) (a) and Mach-Zehnder interferometer (b) evanescent field sensor, indicating resonance shift (δλ) in response to a waveguide effective index change and linewidth (Δλ).

In Eq. (7) the effective length of the ring is defined as $L_{eff} = N \cdot L$ where N is the number of round trips that a light pulse makes inside the ring for its intensity to decay to $1/e^2$ of the initial value. We have used the relation $N = F/\pi$, which is valid for large N.

The transmission spectrum of an MZI is sinusoidal, as shown in Fig. 4b, with a periodicity that is determined by the difference in length and group indices of the two arms. In an MZI sensor, one arm is typically functionalized and used for sensing while the other arm is a reference waveguide. In response to a change in the effective index of the sensor arm $\delta n_{eff,s}$, the spectrum shifts by an amount $\delta\lambda_{MZI}$, as shown in Fig. 4b. In analogy to the resonant grating and ring resonator sensors, it is convenient to define an MZI resonance width $\Delta\lambda_{MZI}$ as one half of the period of the spectrum, as indicated in Fig. 4b. In this case the shift and width of the MZI peaks are given by:

$$\delta\lambda_{MZI} = \frac{\lambda L_s \delta n_{eff,s}}{n_{g,s}L_s - n_{g,r}L_r} \tag{8a}$$

$$\Delta\lambda_{MZI} = \frac{\lambda^2}{2\left(n_{g,s}L_s - n_{g,r}L_r\right)} \tag{8b}$$

The subscripts "s" and "r" in Eq. (8) refer to sensing and reference arms of the MZI, respectively. Again, the sensitivity FOM of an MZI sensor can be calculated:

$$S_{MZI} = \frac{1}{\Delta\lambda_{MZI}}\left(\frac{\delta\lambda_{MZI}}{\delta n_{eff,s}}\right) = \frac{2L_s}{\lambda} \tag{9}$$

Equations (5), (7) and (9) show an interesting common principle for the three configurations of evanescent field sensors considered here, namely that the sensitivity FOM S is proportional to the ratio of the propagation length L of the light in the sensing waveguide and the wavelength λ. In general, for an evanescent field sensor, the total phase change $\delta\phi$ of the light signal caused by attachment of molecules to the surface of a linear waveguide is given by $\delta\phi = (2\pi/\lambda)\delta n_{eff} L$. Since we have found that $S = \delta\lambda/(\Delta\lambda\delta n_{eff}) \propto (L/\lambda)$ we can conclude that the ratio of the induced spectral shift and the linewidth of the resonance is a direct measure of the

phase change $\delta\phi$. The results of this section allow us to compare more clearly the merits of the different sensor configurations. The main advantage of the ring resonator configuration is that the trade off between sample size and sensitivity can be circumvented to some degree, as the effective propagation length L_{eff} can be increased by increasing the finesse F of the ring and without increasing sensor size. However, in addition to the practical difficulties in fabricating high finesse ring resonators, it has been shown that for very sharp resonances, wavelength noise becomes the dominant limitation on sensitivity and our simple assumed scaling of $S \propto (\Delta\lambda)^{-1}$ is no longer justified [9,10]. Balanced MZI sensors, on the other hand can be designed wavelength independent. For MZI sensors made with silicon photonic wire waveguides, densely folded waveguide designs can be used to maximize waveguide length and thus sensitivity for a given sensor area [2]. For the resonant grating sensor, on the other hand, there is no obvious way of reducing the size without decreasing sensitivity. The real advantage of this configuration lies therefore not in ultimate sensitivity for a given sample size but in its simplicity of fabrication and packaging. For many applications this advantage could be crucial.

3. Experimental demonstration

Samples were fabricated from commercial SOI substrates with 0.22 μm thick silicon and 3 μm thick BOX layers. The backside of the wafer was polished and coated with a 9-layer AR coating consisting of alternating films of SiO_2 and Nb_2O_5 to minimize substrate Fabry-Pérot fringes in the reflectivity spectrum of p-polarized light in a wavelength band of λ = 1.5-1.55 μm. The SiO_2 gratings with a thickness of 180 nm and a pitch of 1.24 μm were fabricated by electron beam lithography using hydrogen silsesquioxane (HSQ) resist, which forms SiO_2 upon electron beam exposure. The grating size was 5 mm × 7 mm. For mass production the grating could be produced by other standard lithography tools, such as a UV stepper, or by holography. Figure 5a shows a photograph of a chip with two gratings. A scanning electron microscope (SEM) image of a fabricated HSQ grating is shown in Fig. 5b.

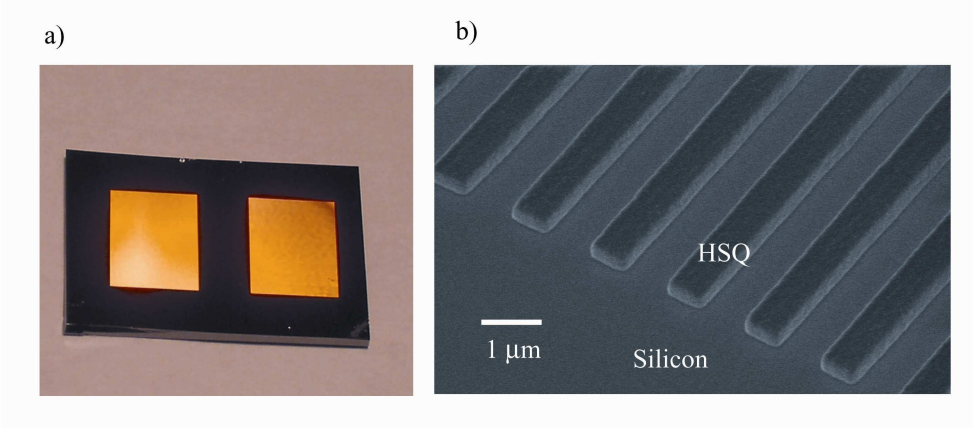

Fig. 5: a) Photograph of an SOI resonant grating sensor chip with two gratings of size 5×7 mm^2. b) SEM micrograph of a SiO_2 grating on the surface of an SOI chip fabricated using HSQ resist and electron beam lithography.

Reflectivity spectra were measured by scanning the wavelength of a tunable laser source over the spectral range of interest. An InGaAs photodetector was used. The angle of incidence of the laser beam was fixed in the optical setup at θ = 45°. To excite the TM mode of the slab waveguide, p-polarized light was used. For a first demonstration of protein sensing we used the biotin-streptavidin model system. First, a reference spectrum was taken in air from a bare untreated grating. The measured guided mode resonance, centered at a wavelength of λ = 1.531 μm with a FWHM of ~5 nm, is shown in Fig. 6a (black curve). The grating surface was

then cleaned with nitric acid and functionalized with an aminopropylmethyldiethoxysilane (APMDES) molecular layer, terminated with biotin molecules, and a second spectrum was taken (blue curve in Fig. 6a). The silanization step was carried out in the gas phase by placing the sample over a vial of the APMDES solution for 20 minutes in a sealed chamber. The biotin termination was added by immersing the sample into 0.1 mg/ml solution of N-hydroxysuccinimide-activated biotin in dimethylformamide for 60 minutes. A wavelength shift of approximately 0.5 nm was observed. Finally, the functionalized sensor was exposed to a 0.1 mg/ml solution of streptavidin in phosphate buffered saline (PBS) solution for 60 minutes. The streptavidin molecules bind selectively to the biotin receptors on the surface. The spectrum was measured again and a ~1 nm shift of the resonance wavelength compared to the silanized surface was observed (red curve in Fig. 6a). The grating surface was dried after the functionalization and protein attachment steps and measurements were taken in air. The experimental results are compared to RCWA calculations of the model structure in Fig. 6b, which show a wavelength shift of ~1 nm for attachment of a 2 nm thick organic layer. The calculated shift is in good agreement with the observed shift caused by the attachment of a ~1.8 nm thick streptavidin layer [2]. The thickness of the APMDES layer was determined by ellipsometry on a test sample to be less than 1 nm thick, consistent with the smaller observed resonance shift of the grating sensor. There is also remarkable agreement between experiment and theory with regard to the resonance width and line shape. The ripples in the spectra are residual Fabry-Pérot fringes arising from the cavity formed by front and back surfaces of the 640 μm thick Si substrate because of the imperfect AR coating. This effect is also included in the calculated spectra of Figure 6b. The center wavelength of the guided mode resonance observed in the experiment is 18 nm shorter than predicted by the RCWA calculations. This shift is well within the wavelength uncertainty expected given the SOI manufacturer's tolerances in specified silicon waveguide thickness. While the measurements for this first experimental demonstration have been taken in air, real time detection of protein attachment from a fluid analyte delivered to the sample using microfluidics is also possible.

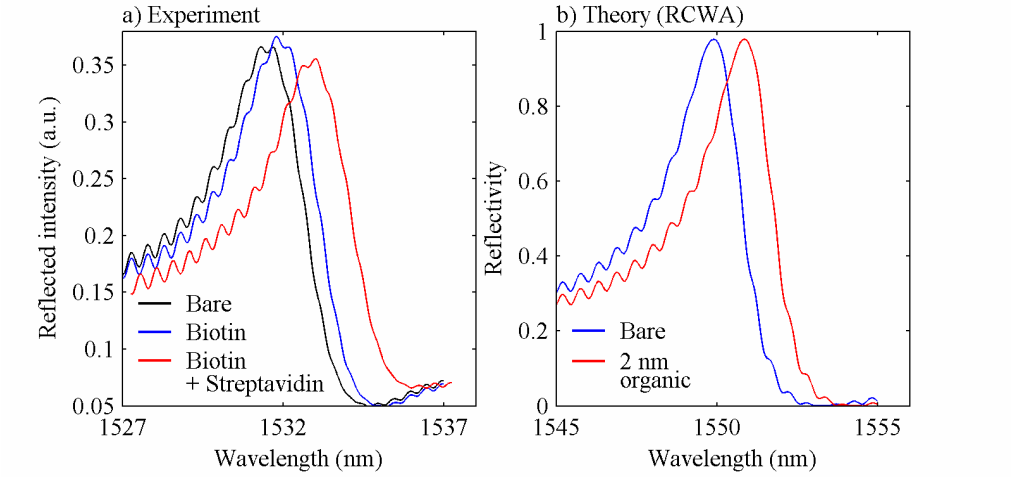

Fig. 6: a) Measurements of guided mode resonance spectra in air for a clean surface, a biotin functionalized surface and after a layer of streptavidin protein is adsorbed. b) RCWA calculation of the reflection spectra for a grating with the structural parameters of the experiment with a clean surface and with an additional organic layer of 2 nm thickness.

After the formation of a protein monolayer the ratio of measured wavelength shift to linewidth was $\delta\lambda/\Delta\lambda \sim 0.2$. This resonance shift is clearly visible in Fig. 6a suggesting that the attachment of a small fraction of a protein monolayer can be detected. In fact, from an examination of the noise floor of our measurements in the current setup, we estimate a limit of

detection of 0.2% of a monolayer of streptavidin. We expect that further sensitivity improvements can be achieved for an optimized grating coupling strength. According to slab waveguide calculations, the change in effective index of a 0.22 μm thick silicon waveguide δn_{eff} caused by attachment of a 2 nm thick organic layer is ~3×10^{-3} for an air cladding and ~1.5×10^{-3} for a water cladding. Equation (5) predicts that for a 7 mm long grating, a ratio of $\delta\lambda/\Delta\lambda$ ~ 10 in air and $\delta\lambda/\Delta\lambda$ ~ 5 in water should be achievable, corresponding to a 25 times improvement in sensitivity in water. This result suggests that the sensitivity FOM in our experiment is limited by the large coupling strength of the grating, which causes a short photon lifetime in the waveguide, rather than by the sample size.

4. Conclusions

We have presented an experimental and theoretical study of SOI resonant grating sensors using 0.22 μm thick silicon waveguides. We used RCWA to calculate a bulk refractive index sensitivity of ~110 nm/RIU and to demonstrate that the resonance linewidth depends strongly on the grating coupling strength. Our theoretical analysis showed that, for an optimized grating coupling strength, the ratio of wavelength shift of the sensor to linewidth is ultimately limited by the grating size. An analogous result was also derived for photonic wire evanescent field sensors in a ring resonator or MZI configuration. While photonic wire sensors can ultimately deliver a better trade off between sample size and sensitivity, resonant grating sensors can exploit the sensitivity of thin silicon waveguides with comparably simple fabrication and packaging requirements. In particular, silicon photonic wire sensors have been shown to be well suited for surface sensing due to the large overlap of the guided mode with the waveguide surface. Since the silicon slab waveguide mode used in our grating sensors has a similar transverse mode profile to the photonic wire waveguides, a comparable surface sensitivity is achieved. Finally, we have provided a first experimental demonstration of an SOI guided mode resonance sensor. A wavelength shift of ~ 1 nm was observed for attachment of a monolayer protein on the sample surface, in excellent agreement with RCWA calculations.